

# Cell Polarity-Driven Instability Generates Self-Organized, Fractal Patterning of Cell Layers

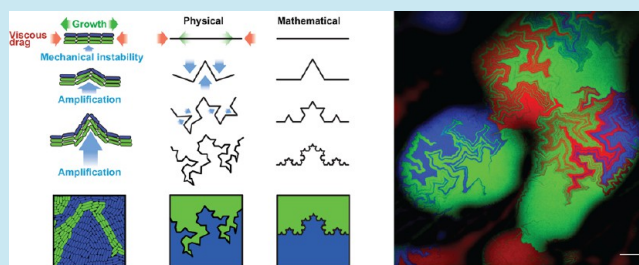
Timothy J. Rudge,<sup>†</sup> Fernán Federici,<sup>†</sup> Paul J. Steiner,<sup>†</sup> Anton Kan, and Jim Haseloff\*

Department of Plant Sciences, University of Cambridge, Cambridge, U.K.

## S Supporting Information

**ABSTRACT:** As a model system to study physical interactions in multicellular systems, we used layers of *Escherichia coli* cells, which exhibit little or no intrinsic coordination of growth. This system effectively isolates the effects of cell shape, growth, and division on spatial self-organization. Tracking the development of fluorescence-labeled cellular domains, we observed the emergence of striking fractal patterns with jagged, self-similar shapes. We then used a large-scale, cellular biophysical model to show that local instabilities due to polar cell-shape, repeatedly propagated by uniaxial growth and division, are responsible for generating

**KEYWORDS:** fractal, self-organization, bacteria, biophysics, GPU, confocal, biofilm, pattern



this fractal geometry. Confirming this result, a mutant of *E. coli* with spherical shape forms smooth, nonfractal cellular domains. These results demonstrate that even populations of relatively simple bacterial cells can possess emergent properties due to purely physical interactions. Therefore, accurate physico-genetic models of cell growth will be essential for the design and understanding of genetically programmed multicellular systems.

Multicellular organisms generate highly organized spatial structures, which are the result of genetic regulation, cellular signaling, and physical forces. Domains of cellular identity are generated by molecular signals (morphogens) that lead to downstream genetic regulation and differentiation. An externally imposed distribution of signals (e.g., a gradient) may give rise to differential cellular responses (ref 1 reviews some of these systems). In other systems, cellular patterning may be self-organized, for example by a reaction-diffusion system (reviewed in ref 2) in which two locally produced, opposing signals interact to spontaneously generate patterning. Colonial organisms, such as bacteria, also self-organize at the population level. They exhibit spatially patterned gene expression,<sup>3</sup> undergo cellular differentiation, and create elaborate morphological structures.<sup>4</sup>

Domains of cell types are propagated by cell growth and division, and the resulting mechanical interactions give rise to particular spatial patterns and morphologies. Genetic regulation leads to cell type-specific mechanical (e.g., adhesion) and geometric (cell shape) properties that contribute to domain shape. These mechanical and geometric effects can give rise to developmental organization, for example, orienting cell polarity<sup>5</sup> and dorsal closure in *Drosophila*.<sup>6</sup> Cell shape has been shown to be critical to several forms of spatial organization in both multicellular organisms<sup>7</sup> and bacterial populations.<sup>8,9</sup> These physical effects on domain shape and size affect signal transmission and change the level of signals each cell observes, e.g., because of position in a morphogen gradient. There is thus a complex interplay between physical and molecular mechanisms that is difficult to decouple in multicellular systems

Synthetic biology has proved useful in both constructing simple novel systems and elucidating existing regulatory networks and mechanisms, most often in bacteria or yeast. Intracellular regulatory networks of varying complexity have been constructed and measured in bulk liquid culture,<sup>10</sup> whole colonies,<sup>11</sup> and in single cells using time-lapse microscopy.<sup>12,13</sup> At the same time, reconstruction and rewiring of natural systems<sup>14–16</sup> has provided insights into the details of gene expression, as well as broader principles of regulatory networks. Populations of bacterial cells have been used to engineer coordination via diffusing signals, for example, to synchronize oscillations,<sup>17–19</sup> and to form simple spatial patterns.<sup>20</sup> These studies, using very simple model systems in which the processes of interest can be isolated and measured, further our understanding of general biological principles and enable their application to engineering.<sup>21</sup>

The complex interaction of cell growth and division with molecular signaling and regulation suggests the use of such simple, abstract model systems to isolate the effects of physical organization on multicellular behavior. Purely physical systems, for example, simple discrete rod-shaped particles, have been shown to spatially self-organize when vibrated or subjected to varying temperatures.<sup>22</sup> Although such experiments have informed our understanding of mechanisms of physical self-organization, such as phase transitions, they lack the most crucial generative mechanisms in multicellular biology: cell growth and division. Bacteria represent perhaps the simplest

Received: March 15, 2013

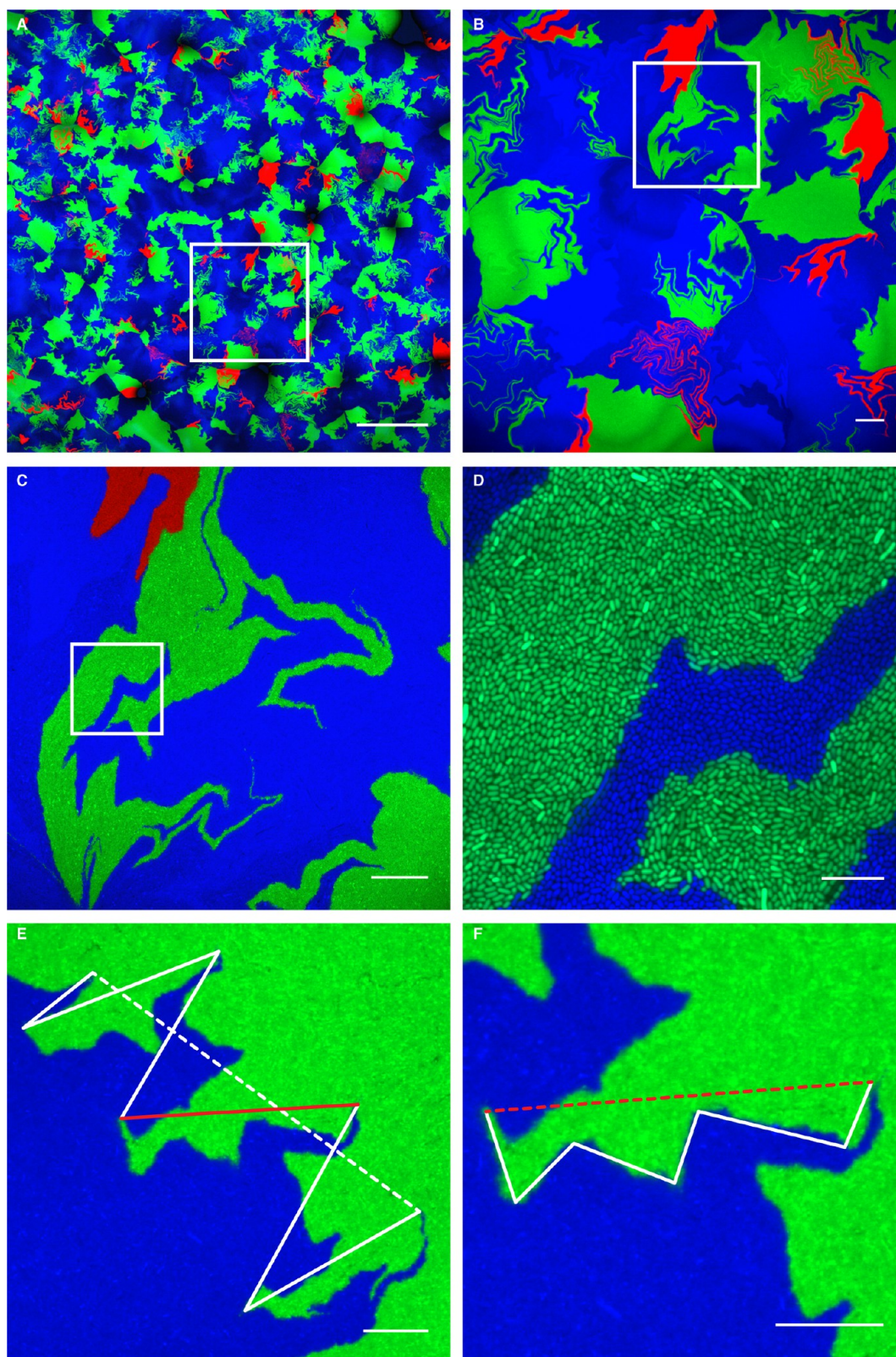


**Figure 1.** Formation of boundaries between growing bacterial populations. (A–D) Surface growing *E. coli* labeled with three different fluorescent proteins: mTurquoise2 (in blue), mRFP1 (in red) and sfGFP (in green). White boxes indicate magnification steps. Scale bars, 1 mm in A, 100 μm in B, 100 μm in C, 10 μm in D. (E, F) Self-similar boundary between two populations of cells (labeled with mTurquoise2 in blue and sfGFP in green). The form of boundaries (solid lines) between colonies (dotted lines) is repeated at smaller scales (F). The red solid line in E represents a smaller boundary analyzed at a lower scale in the left image (red dotted line). Scale bars, 30 μm.

systems in which to study physical organization in growing and dividing cellular populations. Examples of such studies include

aggregation of motile *Bacillus*,<sup>23</sup> swarming of *Escherichia coli*,<sup>24</sup> alignment of dense populations of *E. coli*,<sup>25</sup> and folding of

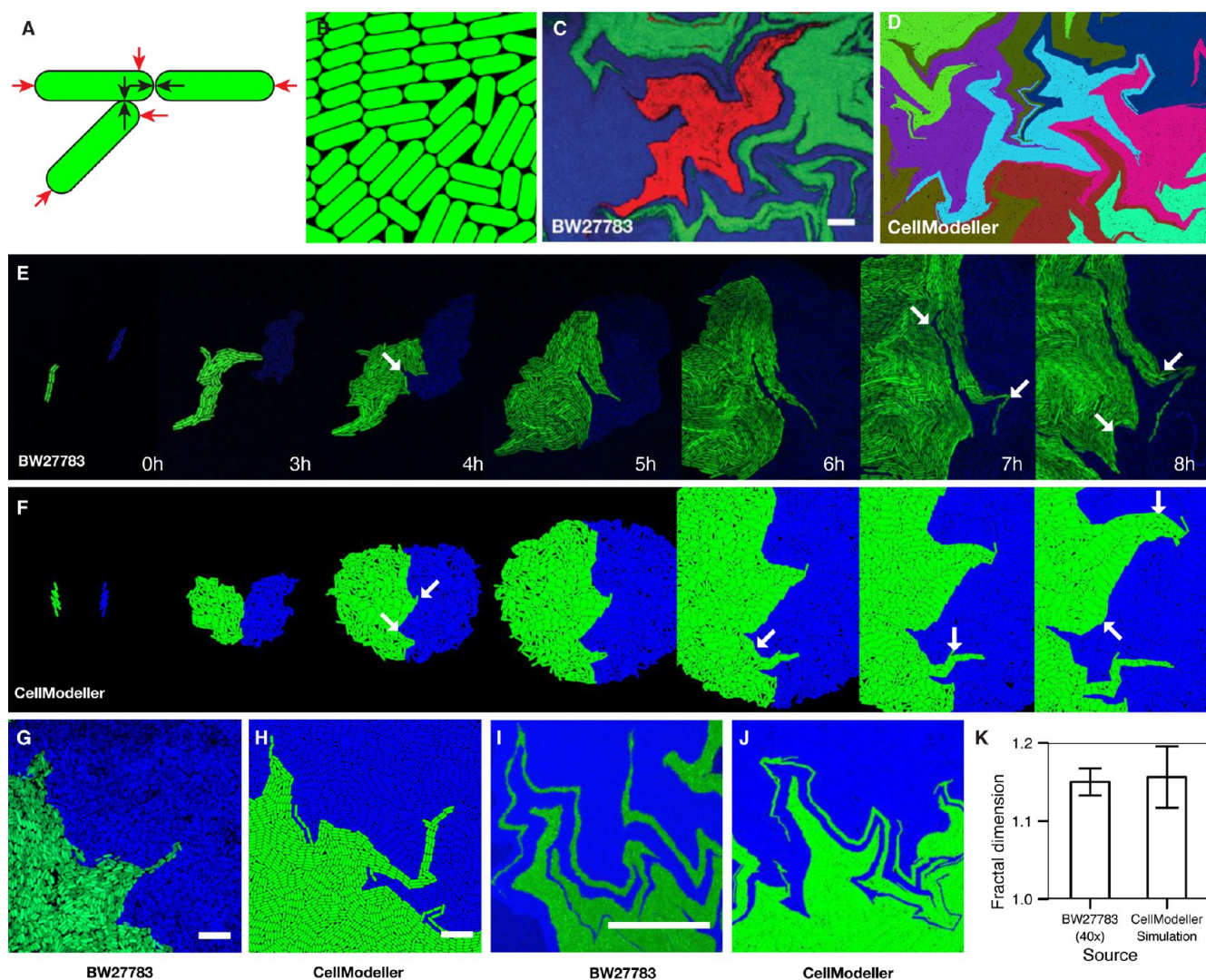


**Figure 2.** A dynamic model of physical interactions between growing and dividing rods gives rise to fractal boundaries. (A) Cells are modeled as growing capsules; growth exerts forces on neighboring cells (black arrows) and is resisted by viscous drag (red arrows). (B) Combined with cell division, this physical system results in arrangements of cells similar to experiments. (C, D) Arrangements of clonal lineages in populations of *E. coli* (C) are reproduced in our bacterial simulator (D), which incorporates only physical interactions between cells and simple growth dynamics. Scale bar, 20  $\mu\text{m}$ . (E) Time-lapse confocal microscopy of the formation of a domain boundary reveals that folding events occur sequentially (arrows), as is reproduced by our biophysical model (F). Scale bars, 10  $\mu\text{m}$ . (G–J) Comparison of *E. coli* populations (G, I) with simulations (H, J) showed similar complex boundary features. (K) Comparison of the fractal dimensions of boundaries within populations of *E. coli* (40 $\times$  confocal images), and simulations show no significant difference ( $p = 0.696$ ,  $n = 10$ , Welch's  $t$ -test).

*Bacillus subtilis* biofilms.<sup>26</sup> In particular, nonmotile, nonbiofilm forming, quorum sensing deficient strains of *E. coli* exhibit little or no molecular spatial coordination, and their growth can be predicted by simple physical models.<sup>27</sup>

We used layers of surface-growing bacteria as a model of physical organization of multicellular systems in the absence of significant molecular coordination. Bacteria grow extremely rapidly and are easily maintained in live imaging conditions, physically constrained, or subjected to varying environmental conditions. Their small scale also means that a typical 12 h growth period can yield thousands of colonies on a single plate. We were thus able to use high-resolution confocal microscopy, with populations constrained to grow in layers, to observe the development of large numbers of cellular domains. As outlined above, genetic manipulation of bacteria is well established, there are a wealth of genetic elements and tools, and they can be applied in a matter of days. Accurate mathematical and

computational models of bacterial biophysics<sup>27</sup> and genetic regulation have also been developed. This combination of speed and ease of manipulation, and accurate modeling, make bacteria an attractive model for engineering and studying multicellularity. To this purpose, fluorescent markers were used in *E. coli* and *B. subtilis* to create cellular domains, which were either prespecified, or spontaneously assigned by plasmid segregation. We used confocal microscopy to observe these artificial cell-type domains as they were propagated by cell growth and division.

## RESULTS AND DISCUSSION

**Rod-Shaped *E. coli* Form Fractal Domains.** We created initial conditions in which synthetic cell-type domains are prespecified in otherwise isogenic *E. coli* populations. Cell types were marked by transforming *E. coli* with plasmids expressing different fluorescent proteins. Agar plates were then seeded

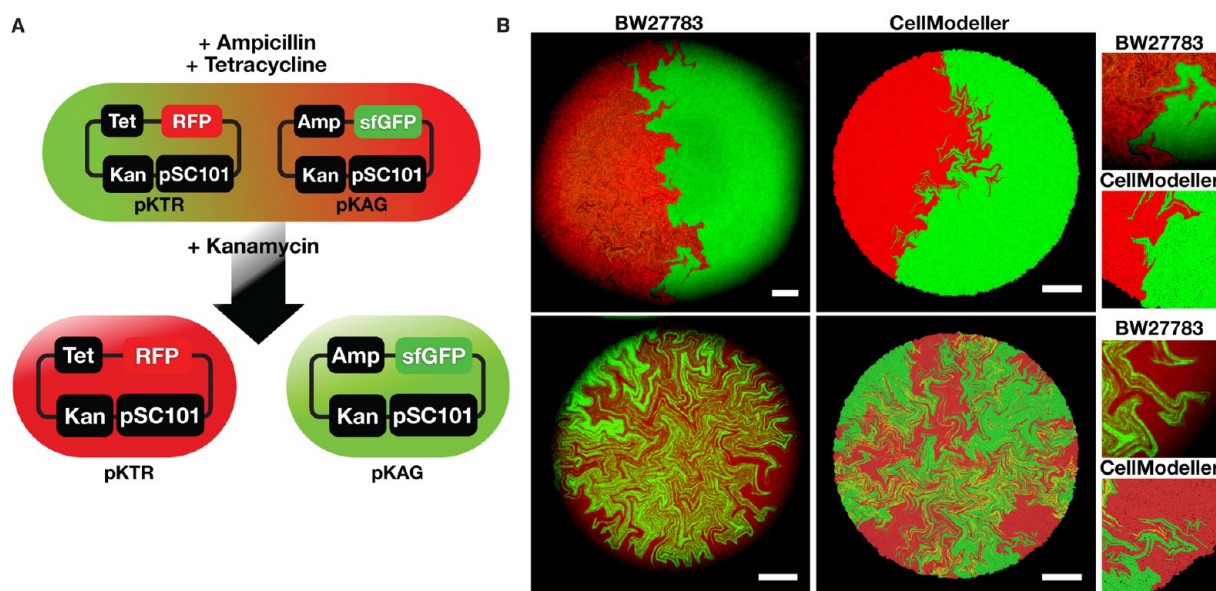


**Figure 3.** Marking and measurement of lineage domains within colonies. (A) Schematic representation of the cell lineage-marking system pKAG/pKTR. Plasmids expressing red (pKAG) and green (pKTR) fluorescent proteins are maintained in the cell by the presence of tetracycline and ampicillin antibiotics. Labeling of different lineages is obtained by the asymmetric segregation of pKAG and pKTR plasmids when only kanamycin is present in agar plates. (B) Left, confocal images of cell lineage distribution in *E. coli* colonies; right, formation of self-similar boundaries in CellModeller simulations of cell lineage markers in growing colonies. Segregation in CellModeller was obtained by random partitioning of plasmids. Scale bars, 100  $\mu\text{m}$ . Insets show 4 $\times$  magnified details of features of experimental populations and simulations.

with equal densities of cells of each type, such that distinct domains formed from spatially separated single cells. These domains grew to be adjacent, enabling examination of their physical interactions. High resolution confocal microscopy was used to image the plates after approximately 12 h, revealing striking jagged patterns of cellular domains (Figure 1A–D). The boundaries between these domains were punctuated by repeated angular folds, giving a self-similar fractal appearance observable at many scales from micrometers to millimeters (Figure 1E,F).

We measured the fractal dimension of the boundaries of multiple domains to be  $1.23 \pm 0.041$  (Figure S1A,B, Supporting Information), indicating significant self-similarity ( $p = 1.1 \times 10^{-8}$ , one-sided  $t$ -test). Accurate quantification of fractal dimension from experimental data is difficult, because of limitations on resolution and scale. However, it is a useful comparative measure, and in this study we use it only to characterize the nature of the observed patterns and the effects of different conditions on them. Since these cell-types were isogenic apart from fluorescent protein coding sequence, it is unlikely that their interaction is regulated by signaling or other coordination mechanisms. To eliminate differential growth due to the cells expressing different fluorescent proteins as an underpinning physical mechanism, we examined the growth of each strain in liquid culture and found no significant differences in growth rates (two-tailed  $t$ -test,  $p = 0.7281$ , Figure S1C, Supporting Information).

The apparent lack of genetic coordination and the results of previous studies on ordering of dense *E. coli* populations suggested that the observed patterns could be the result of physical effects of individual cell growth and division. *E. coli* is a rod-shaped bacterium, roughly cylindrical with hemispherical ends, forming a capsule that exhibits extremely regular growth and division dynamics.<sup>28</sup> Vegetative growth consists of exponential expansion along the long axis with cell diameter remaining roughly constant<sup>28</sup> (Figure S2A,B, Supporting

Information). Division precisely bisects the cell across the long axis.<sup>28,29</sup> The average doubling time and the average length at division are both constant, with low variance, over hundreds of generations.<sup>29</sup> Molecular and genetic factors such as quorum sensing, differentiation, and nutrient depletion may affect growth dynamics.<sup>4,30,31</sup> However, in the absence of such effects, the population can be approximated as a physical system of rigid expanding and dividing capsules. We used our computational modeling framework, CellModeller,<sup>27</sup> to investigate whether such a system of locally interacting, growing and dividing capsules could generate the observed fractal domain boundary shape.

**Computational Modeling of Biophysics of Rod-Shaped Bacterial Populations.** We modeled a physical system of expanding and dividing cells on the basis of the following assumptions: (1) Cells are rigid elongating capsules.<sup>28</sup> (2) Viscous drag dominates inertia; cells are nonmotile and move only when subjected to a force.<sup>32</sup> (3) The distribution of cell lengths at division is constant, and each cell divides in half.<sup>28,29</sup> Each cell's target length was chosen at birth and was uniformly distributed in an interval based on cell length measurements (Figure S2A, Supporting Information). (4) Each cell's unconstrained growth rate is proportional to its length.<sup>29</sup> (5) Growth is constrained by forces between cells and from viscous drag (Figure 2A). The ratio of the work required to constrain growth to the work required to move a cell is defined by a parameter  $\gamma$ .

This model will generate lines or files of cells due to the axial alignment of growth and division. It will also generate compressive forces due to the opposition of viscous drag to cell growth. These compressive forces will increase as the cell file grows. Axial alignment after cell division is not exact because of, for example, imperfections in shape or Brownian motion. In our model, we simulate this by slightly perturbing daughter cell orientations, creating small local asymmetries. As in classical beam theory, these small asymmetries in cell

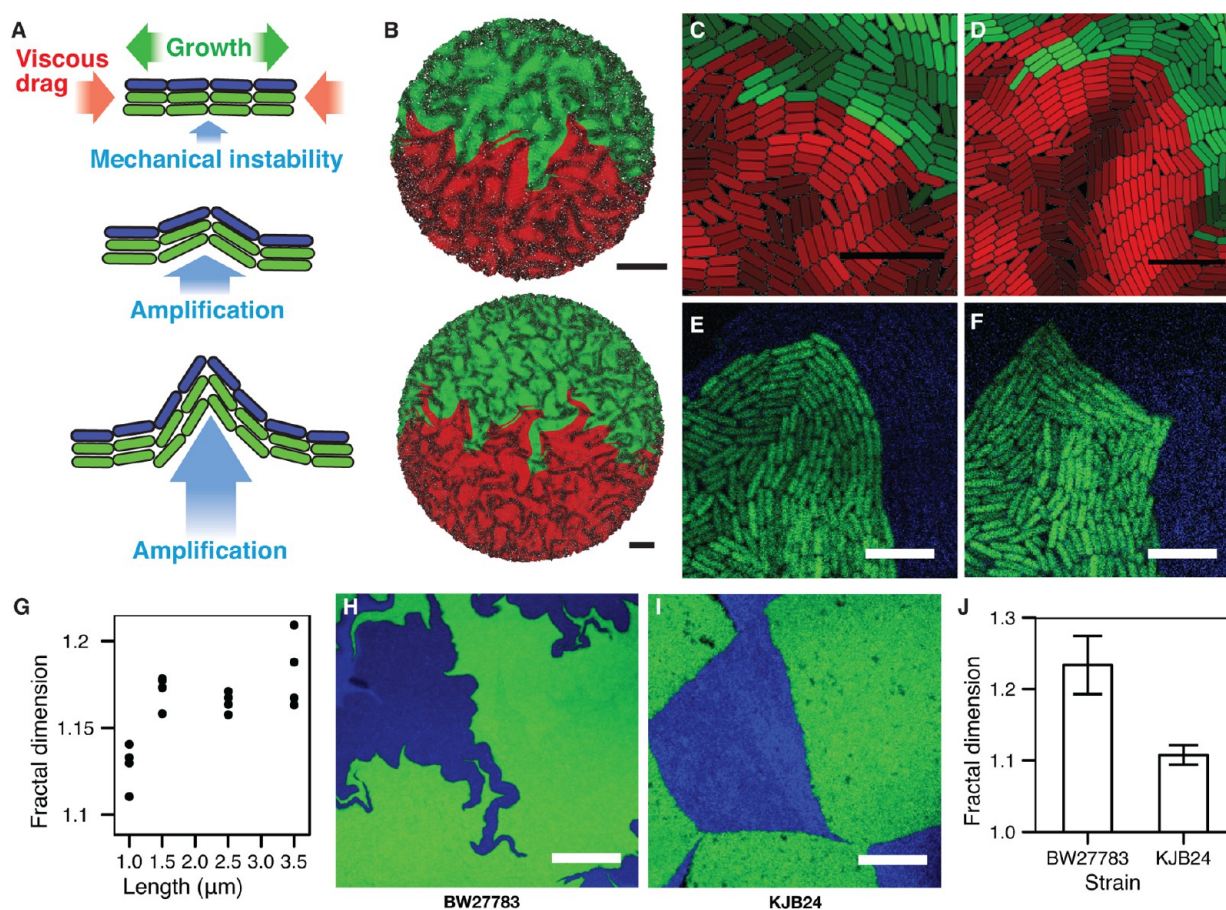


**Figure 4.** Self-similar boundary morphology is an emergent property of rod-shaped cells. (A) A single iteration of the recursive process that produces the buckling due to mechanical instability. In one iteration, compressive forces lead to a similar folding of files of cells. (B) Cell alignment measure,<sup>8</sup> ranging from 0 = unordered, to 1 = fully aligned for two lineages (red, green), are shown as intensities (black = 0, red/green = 1) at two successive time-points. Regions of ordered cells develop that seem to have a characteristic scale. Scale bars, 100  $\mu\text{m}$ . (C–F) Ordered regions fold (as seen in two successive time-points), leading to self-similar boundary shape in simulations (C, D) and in confocal micrographs (E, F). Scale bars, 10  $\mu\text{m}$ . (G) Reduction of cell length, to the point of being initially spherical ( $l = 2 \mu\text{m}$ ), leads to reduction of self-similarity as measured by fractal-dimension. (H, I) Boundaries in populations of spherical cells KJB24 (I) are smoother and show limited self-similarity compared with rod-shaped cells BW27783 (H). Scale bars, 100  $\mu\text{m}$ . (J) Fractal dimension measurements of populations of rod-shaped and KJB24 spherical cells show a significant reduction in the mutant strain ( $p = 1.625 \times 10^{-6}$ ,  $n = 10$ , Welch's  $t$ -test).

alignment should be unstable above some critical level of compressive force, leading to buckling of cell files. Further cell growth and division will cause the new files to expand and should cause this process to repeat each time the local compressive forces become large enough, suggesting that self-similar patterns might be produced.

In order to solve this model for large numbers of cells, we apply a growing, constrained rigid-body dynamics method, which simulates 3-dimensional growth.<sup>27</sup> Note that in our experiments cell growth was largely in the plane of the substrate surface, especially when constrained by a coverslip for high-resolution imaging, and so we limited our simulations to two dimensions (Figure 2B and Figure S2C, Supporting Information). The simulations were performed with a target cell length uniformly distributed in the interval 4.5–5.0  $\mu\text{m}$  based on measurement of *E. coli* grown in our experimental setup (Figure S2A,B, Supporting Information). We initiated simulations with multiple, distinctly marked founder cells, and allowed them to grow to approximately 100 000 cells in total.

The results reproduced the characteristic cell alignment and domain shapes observed in experimental *E. coli* populations (Figure 2C,D). The development of a boundary between two

growing domains of cells was tracked with a confocal microscope over time and compared to a simulation with similar initial conditions (Figure 2E,F). In both the model and experiment, marked boundaries underwent repeated and sequential folding (arrows in Figures 2E,F). The simulations produce complex features characteristic of observed clonal domains (Figure 2G–J). The fractal dimension of simulated boundaries between domains was measured and found to be consistent with confocal micrographs of *E. coli* populations (Figure 2K, Figure S2D,E, Supporting Information). Although the detailed physics of *E. coli* may be complex, this simplified model of local interactions between cells produces an emergent fractal morphology that is comparable to measurements of surface-growing *E. coli*. This result suggests a critical role for physical interactions in the observed patterns of cellular domains.

**Marking and Measurement of Lineage Domains within Colonies.** If fractal boundaries between prespecified domains are formed primarily by physical phenomena, it would be reasonable to expect that similar boundaries might form between domains initiated from single cells within colonies. We created a genetic tool for initiating such domains and marking

subsequent lineages with different fluorescent proteins (Figure 3A). *E. coli* bacteria were transformed with two plasmids carrying the same origin of replication conferring kanamycin resistance (Figure 3A). Each of these plasmids provides expression of a different fluorescent protein and also carries a second resistance marker (tetracycline or ampicillin). Growing cells in the presence of both tetracycline and ampicillin ensured maintenance of both plasmids in every cell. Cells were then transferred to agar for imaging with selection for kanamycin resistance only, permitting spontaneous loss of one of the two plasmids, and yielding fluorescently labeled lineages. When grown in the same conditions as used for prespecified domains, these colonies produced abutting lineages with the same characteristic fractal geometry (Figure 3B).

We then used CellModeller to simulate plasmid partitioning in a growing colony. We either marked the lineages of cells from the division of the first cell (to model early segregation, see the video in the Supporting Information), or explicitly modeled plasmid segregation by random partitioning (Supporting Information). Founder cells each carried four plasmids, two each of green and red. At division, each plasmid was duplicated, retaining its color. The pool of eight plasmids was then randomly divided between the two daughter cells, with equal probability of being inherited by either daughter. At each division there is then a finite probability of segregation, which increases on average over time. These two models of segregation closely reproduced the observed fractal patterns (Figure 3B), including detailed features of cell arrangements that are not obvious from the model formulation.

#### Effect of Cell-Shape on Domain Boundary Geometry.

Previous studies of *E. coli* in microfluidic chambers have shown ordering effects due to axial cell shape and growth. The physical forces between cells in a population are highly dependent on cell shape and oriented growth. In particular, axial shapes will produce locally anisotropic distributions of forces. Our biophysical model suggests that these anisotropic, axially aligned forces are the compressive forces that lead to instabilities and cause folding of boundaries (Figure 4A). Alignment of cell axes also contributes to the anisotropy of forces in the biofilm, amplifying further the effects of buckling (Figure 4B–F).

The degree of cell polarity should therefore impact on domain boundary shape, and so we used our computational model to examine the effect of changing the aspect ratio of the capsules. We simulated populations with 1  $\mu\text{m}$  diameter capsules of different lengths at division (from 2–5  $\mu\text{m}$ ). For the shortest length (2  $\mu\text{m}$ ), newly formed daughter cells were spherical. We found that the degree of self-similarity as measured by fractal dimension decreased with reduced cell length (from  $1.18 \pm 0.021$  for cells 4.5–5  $\mu\text{m}$  at division to  $1.13 \pm 0.013$  for cells 2–2.14  $\mu\text{m}$  at division; Figure 4G; Figure S3A–D, Supporting Information).

These simulations show that emergence of fractal ordering of cellular domains is dependent on polarity of cell shape, growth and division. To test this result *in vivo* we examined populations of the *E. coli* mutant strain KJB24 (Figure S3E–H, Supporting Information). This strain has a stop codon mutation in the cell wall protein RodA, causing it to form spherical cells;<sup>33</sup> a second mutation confers stability by increasing transcription of *ftsQAZ*.<sup>34</sup> It is viable at 37 °C and maintains a regular cell division cycle, having an apparently functional Min protein system that locates a partial z-ring (FtsZ) across the center of the cell.<sup>33</sup> It is therefore an ideal control for the effects of rod-

shaped polar growth. Following the same procedures as used for rod-shaped cells, we studied prespecified cellular domains in KJB24 populations. Confocal microscopy (Figure 4H,I) revealed that domain boundaries were essentially smooth, and fractal dimension measurement confirmed this (reduced from  $1.23 \pm 0.041$  for rod-shaped cells to  $1.11 \pm 0.014$  for spherical cells,  $p = 1.625 \times 10^{-6}$ ,  $n = 10$ , Welch's *t*-test; Figure 4H–J; Figure S3I,J, Supporting Information). Similar results were found when cellular domains spontaneously generated by plasmid segregation were imaged (Figure S3K, Supporting Information). Minimizing the polarity of cell-shape, growth and division therefore resulted in smooth boundaries without the characteristic self-similar appearance of rod-shaped cells, and a corresponding significant reduction in the measure of self-similarity.

In this study we report the formation of patterns in layers of surface growing *E. coli* that have a striking fractal appearance. We used high-resolution confocal microscopy and image analysis to quantify arrangements of cells, capturing multiple scales and tracking development over time. The fractal boundaries were observed as multiple bacterial colonies grew together to form a confluent film. Further, we constructed a system for triggering the segregation of incompatible plasmids that encoded different color fluorescent proteins. This allowed the formation of distinct, genetically marked clonal domains within single colonies, which could be followed using high-resolution microscopy. We observed the production of fractal boundaries between the populations of marked cells. Using CellModeller, a recently developed GPU-accelerated computational model,<sup>27</sup> we reproduced the observed fractal patterns in simulated colony-scale populations using a few simple assumptions. The cells were modeled as rigid elongating capsules, which were programmed to grow and then divide when they reached a particular target length. Cells were nonmotile and only moved when subjected to force. Growth of the cells was constrained by viscous drag and forces resulting from intercellular interactions. These simple growth behaviors and physical interactions were sufficient to generate the observed fractal domains, in the complete absence of any extrinsic genetic interactions between the cells.

In separate *in vivo* experiments, we also observed qualitatively similar boundaries in populations of the rod-shaped bacterium *Bacillus subtilis* (Figure S1D, Supporting Information), suggesting that the generation of fractal boundaries is a general property of growing rod-shaped cell populations. The computer models predicted that loss of rod-shape would effectively reduce the fractal morphology. We confirmed this prediction *in vivo* by using a rodA– mutant of *E. coli* that forms spherical-shaped cells. Growth of the rodA– cells resulted in the formation of smooth boundary interfaces between both adjacent colonies and clonal sectors within a colony. The results confirmed that fractal shaped domains are an emergent property of the interactions between growing rod-shaped cells. In our models, the uniaxial growth of rod-shaped cells results in the formation of cell files. However, compressive forces build up in cell files due to viscous drag, and small asymmetries in cell alignment cause instabilities to propagate, causing buckling or folding of cell files (Figure 4A–F). The close correspondence between our simulations and observations strongly suggest that the same mechanism is at work in bacterial populations. To illustrate, consider a single rod-shaped cell growing on flat agar substrate. At the scale of bacterial cell size, viscous forces dominate inertia, and the cell must generate force equal to the

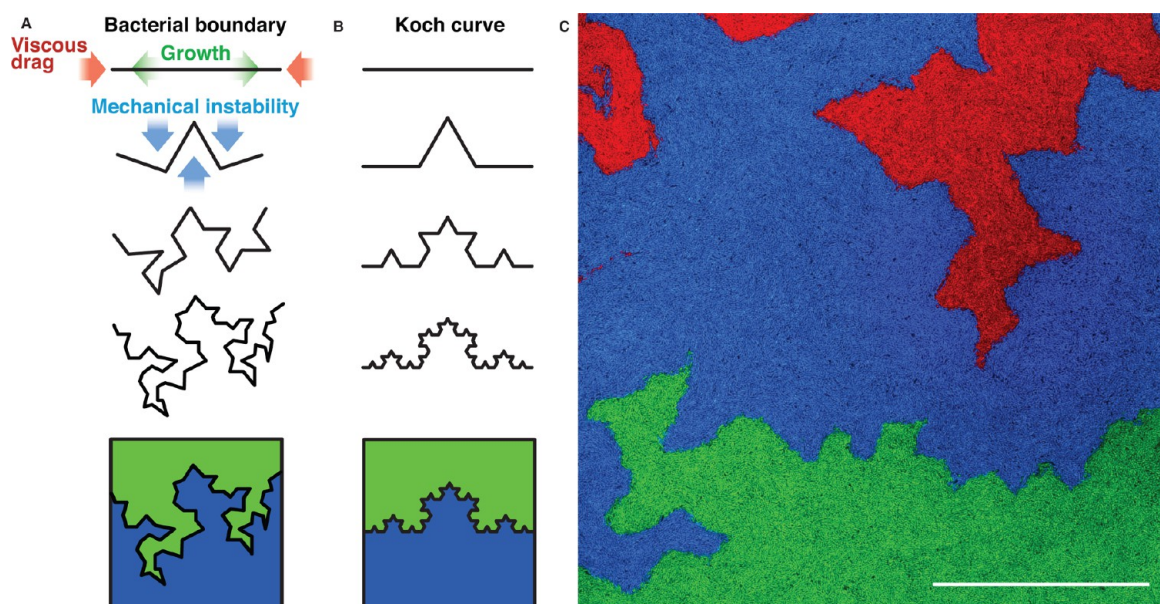


**Figure 5.** Schematic representation of fractal boundary emergence in bacterial populations due to local mechanical instabilities generated by uniaxial growth, division, and viscous drag. (A) Physical generation of fractal boundaries in bacterial populations follows a similar process to (B) mathematical generation of the Koch fractal. (C) Surface growing *E. coli* labeled with three different fluorescent proteins: mTurquoise2 (in blue), mRFP1 (in red), and sfGFP (in green). Scale bars, 100  $\mu\text{m}$ .

drag exerted on it by the substrate in order to grow, subjecting it to a compressive force. If the cell grows axially and divides perpendicular to its axis, then growth and division produces a file of cells also under compression. The total compressive force at any point along the line is the sum of all viscous drag forces to each end of the file from that point. Hence as the cells grow the compressive forces increase and are distributed with a maximum at the midpoint of the file. There is a critical level of this maximum compression at which forces due to imperfections in cell alignments will overcome surrounding constraints, and the file will buckle (Figure 4A).

Boyer et al. observed cellular buckling in small populations of *E. coli* grown in microfluidic chambers and proposed it as an explanation of their observation of cellular reordering.<sup>8</sup> In their experiments, initially well-ordered files of cells, measured using a local alignment parameter, were seen to break alignment at a critical file length. This work was carried out in small devices (<1 mm) and so was not able to show the effects of propagation by growth on the scale presented here. We calculated a measure of local alignment for our simulations, and the results highlighted distinct regions of ordered cells (Figure 4C,D). These regions broke order by folding and subsequently split into multiple subdomains as the population grew. This folding occurred across the population. When it occurred at a clonal boundary, it caused the shape of that boundary to similarly fold (Figure 4C,D). The same phenomena was evident in time-lapse confocal micrographs of *E. coli* populations (Figure 4E,F).

Thus uniaxial growth of cells and cell division repeatedly generate buckling instabilities that cause locally ordered domains of cells to split. As the new domains expand, the same process repeats. This iteration is very similar to the processes that generate fractal curves, such as the Koch curve generated by repeated elongation and buckling of a line (Figure 5). In a physical system such as that presented here, spatial constraints and the forces arising from surrounding cells make

the process less regular (Figure 5), but the principle is the same.

The results presented here demonstrate fractal cellular domain shapes that are generated by physical interactions between cells undergoing polar growth. Cell-polarity driven instabilities are repeatedly generated by division and propagated by growth to generate self-similar geometry. This is an example of a self-organized spatial patterning mechanism, where bacterial cells are physically interacting in the absence of genetically encoded patterning information. Our results highlight the potential for emergent properties in even the simplest of interacting cellular populations. Further, we have demonstrated that CellModeller can recapitulate this kind of emergent behavior *in silico*, in large-scale cellular models (>10<sup>5</sup> cells).

The engineering of patterning and fate in cell populations remains a major goal of synthetic biology. The young field has already seen experiments to produce patterns<sup>20</sup> and coordinate oscillations<sup>18</sup> across bacterial films and to reprogram gene expression at the edges of cell cohorts.<sup>35</sup> Potential applications range from artificial organization of biofilms for enhanced catalysis, to the engineering of artificial tissues and organs in multicellular organisms. There are a wide range of potential benefits that would arise from ability to engineer the flow of metabolites through specialized cell populations and storage of products in harvestable form. Bacteria provide a simple and tractable chassis for testing such prototype multicellular systems with self-organizing behavior. However, as we see even in simple multicellular systems, the interplay between genetic programs and the physics of growth will play a major role in fashioning the ultimate form of a multicellular assemblage. Efficient physico-genetic modeling tools like CellModeller will facilitate the *in silico* design and testing of genetic circuits that incorporate intercellular communication and logic.

## METHODS

**Microbial Strains and Growth Conditions.** *E. coli* and *B. subtilis* strains (see Table S1, Supporting Information) were

cultured in LB liquid medium or LB agar (1.5% w/v) supplemented with kanamycin (50  $\mu\text{g mL}^{-1}$ ), ampicillin (100  $\mu\text{g mL}^{-1}$ ), tetracycline (5  $\mu\text{g mL}^{-1}$ ), or chloramphenicol (5  $\mu\text{g mL}^{-1}$ ) when necessary. For imaging experiments, cells were grown overnight at 37 °C in 5 mL of LB liquid medium to an optical density at 600 nm ( $\text{OD}_{600}$ ) of 1.5 ( $\approx 16$  h) and diluted 1:1000 into fresh liquid medium. 100  $\mu\text{L}$  of the dilution was plated onto LB agar plates containing 50  $\mu\text{g mL}^{-1}$  of kanamycin. For images taken with a 40 $\times$  oil immersion objective, coverslips were placed carefully on the plates immediately after inoculation. Images were acquired for analysis after approximately 12 h growth at 37 °C. For time lapse imaging, a coverslip was placed on top of the agar, and plates were imaged on a heated microscope stage held at 37 °C. Images were taken at 1 h intervals. For segregation experiments, cells were grown overnight at 37 °C in 5 mL of LB liquid medium containing 100  $\mu\text{g mL}^{-1}$  of ampicillin and 5  $\mu\text{g mL}^{-1}$  of tetracycline and then diluted 1:1000 into fresh liquid medium containing 50  $\mu\text{g mL}^{-1}$  of kanamycin. 100  $\mu\text{L}$  of the dilution was plated onto LB agar plates containing 50  $\mu\text{g mL}^{-1}$  of kanamycin and imaged after growth. To measure growth rate in fluorescent strains, we grew fluorescent *E. coli* strains in a 96-well plate reader and measured  $\text{OD}_{600}$  every 10 min.

**Plasmids.** Plasmids are listed in Table S2 (Supporting Information) and were constructed by the method of Gibson et al.<sup>36</sup> *E. coli* plasmids have fluorescent proteins expressed from promoter R0010 from the Registry of Standard Biological Parts (Registry), translation initiated with ribosome binding site (RBS) B0034 (Registry), and have transcripts terminated by terminator B0010 (Registry). *B. subtilis* plasmids have fluorescent proteins expressed from promoter  $P_{\text{SPO1-26}}$  from *Bacillus* phage SPO1 with transcription terminated by terminator B0012 (Registry). The efficient *gsiB* RBS was used to drive translation of fluorescent proteins.<sup>37</sup> To increase expression in *B. subtilis*, each fluorescent protein coding sequence was modified by the addition of the first 24 base pairs of the *comGA* coding sequence from *B. subtilis*.<sup>38</sup>

**Microscopy.** Confocal microscopy was performed with a Leica TCS SP5 confocal laser scanning microscope equipped with 2.5 $\times$  air, 10 $\times$  air and 40 $\times$  NA 1.25 oil-immersion objectives. sfGFP was excited at 488 nm (argon ion laser), mTurquoise2 at 458 nm (argon ion laser), mKate2 at 561 nm (DPSS laser) and mRFP1 at 561 nm (DPSS laser). Fluorescence emission was detected at 505–530 nm for sfGFP, 465–480 nm for mTurquoise2, 610–650 nm for mKate2 and 606–635 nm for mRFP1. Multichannel images were merged in ImageJ. Unedited images were used for analysis. For time lapse experiments, images were acquired every 1 h. Images were created by manually merging a z-stack in Adobe Photoshop, and image levels were adjusted for presentation.

**Image Analysis.** Images were processed and analyzed using the Fiji distribution<sup>39</sup> of ImageJ.<sup>40</sup> For boundary identification images were blurred by convolution with a Gaussian kernel and thresholded to give a binary image. Binary images were outlined and skeletonized using built-in ImageJ operators and manually edited when necessary. Euclidean distance metric fractal dimension<sup>41</sup> was calculated using a custom Python script for Fiji with distance thresholds of 1, 2, 3, 4, 6, 8, 12, 16, 24, 32, 48, 64, 92, 128, and 184 pixels. Cell dimensions were measured using ImageJ's line measurement tool. Approximately 350 cells were measured in a single image acquired using 40 $\times$  oil

immersion objective. Distributions of measured lengths and widths are shown in Figure S2A,B (Supporting Information).

**Plate Fluorometry.** For plate fluorometry, cells were grown overnight at 37 °C in 5 mL of M9 minimal medium supplemented with 0.4% w/v glucose and 0.2% w/v casamino acids to an  $\text{OD}_{600}$  1.5 (approximately 12 h), diluted 1:1000 into fresh liquid medium, and 200  $\mu\text{L}$  of culture was added to each well of a black 96-well microplate with clear base (Greiner). A BMG Fluostar Omega plate reader was used to measure optical density at 600 nm every 10 min at 37 °C. Between readings plates were shaken at 200 rpm. Five replicates for each of the strains were used.

**Computational Modeling.** Computational modeling was performed using CellModeller.<sup>27</sup> Simulations were executed on a Hewlett-Packard Z800 workstation with an NVIDIA Quadro FX5800 graphics card. On the basis of measured cell dimensions (Figure S3, Supporting Information), simulations were performed with cells of radius 0.5  $\mu\text{m}$ , and length at division uniformly distributed in the interval 4.5–5  $\mu\text{m}$ . To examine the effect of rod aspect ratio, the mean length at division was varied, but the coefficient of variation maintained. At the smallest division length, cells divided into two spheres of radius 0.5  $\mu\text{m}$ . In order to account for imperfections in alignment, cell orientations were perturbed with 0.1% uniformly distributed noise after each division. Simulations were parametrized by the ratio of growth forces to viscous drag forces ( $\gamma$ ). Varying  $\gamma$  did not qualitatively change the patterns observed but did affect their scale. Since this parameter is not amenable to measurement, we chose  $\gamma = 25$  to best reproduce the observed patterns. Simulations for measurement of fractal-dimension were initiated with two distinctly marked founder cells located 20  $\mu\text{m}$  apart. More complex initial cell arrangements were simulated by placing a 3  $\times$  3 grid of founders with 16  $\mu\text{m}$  spacing. Local alignment order parameter used by Boyer et al.<sup>8</sup> was calculated within a given radius of each cell. This scalar parameter is found for cell  $j$  at position  $\mathbf{x}_j$  by summing weighted contributions pairwise over the other cells in the colony to obtain the following:

$$\eta_j = \left( \frac{\sum_k \rho_{jk} \cos 2\theta_{jk}}{\sum_k \rho_{jk}} \right)^2 + \left( \frac{\sum_k \rho_{jk} \sin 2\theta_{jk}}{\sum_k \rho_{jk}} \right)^2$$
$$\rho_{jk} = \Theta(3\lambda - |\mathbf{x}_j - \mathbf{x}_k|) \times \exp\left(-\frac{(\mathbf{x}_j - \mathbf{x}_k)^2}{2\lambda^2}\right)$$

where  $\Theta$  is the Heaviside step function, the sums on  $k$  are over all cells in the colony, and  $\theta_{jk}$  is the angle between cell  $j$  and cell  $k$ . The weighting is used to measure alignment correlations locally, with  $\lambda$  being the length scale over which correlations are averaged, which was set to 10  $\mu\text{m}$ .

## ■ ASSOCIATED CONTENT

### 📄 Supporting Information

Supporting tables, figures, and video file (.QT). This information is available free of charge via the Internet at <http://pubs.acs.org/>.

## ■ AUTHOR INFORMATION

### Corresponding Author

\*E-mail: [jh295@cam.ac.uk](mailto:jh295@cam.ac.uk).

### Author Contributions

<sup>†</sup>T.J.R., F.F., and P.J.S. contributed equally to this work. T.J.R., F.F., and P.J.S. performed the experimental work and computer modeling of bacterial cell growth, and with A.I.K. performed data analysis. All authors contributed to discussion and writing of the manuscript.

### Notes

The authors declare no competing financial interest.

### ACKNOWLEDGMENTS

The authors wish to thank K. Gerdes and A. Fenton (Newcastle University) for providing *E. coli* strain KJB24; M. Jones (University of Cambridge) and J. Minshull (DNA2.0) for advice on mTurquoise2; H. Ghareeb (Göttingen University), T. W. J. Gadella, and J. Goedhart (University of Amsterdam) for providing mTurquoise2 DNA; J. Lichtman, J. Sanes, and D. Cai (Harvard University) for providing mKate2 DNA; and L. Tsimring for helpful discussion. This research was supported by a joint EPSRC and NSF research grant (EP/H019162/1) to J.H. T.J.R. is supported by a Microsoft Research Studentship, F.F. by Gates Cambridge Scholarship, P.J.S. by a Cambridge International Scholarship, and A.K. by a Microsoft Research/BBSRC CASE Studentship.

### REFERENCES

- (1) Kicheva, A., Cohen, M., and Briscoe, J. (2012) Developmental pattern formation: insights from physics and biology. *Science* 338, 210–212.
- (2) Kondo, S., and Miura, T. (2010) Reaction-diffusion model as a framework for understanding biological pattern formation. *Science* 329, 1616–1620.
- (3) McLoon, A. L., Kolodkin-Gal, I., Rubinstein, S. M., Kolter, R., and Losick, R. (2011) Spatial regulation of histidine kinases governing biofilm formation in *Bacillus subtilis*. *J. Bacteriol.* 193, 679–685.
- (4) Branda, S. S., González-Pastor, J. E., Ben-Yehuda, S., Losick, R., and Kolter, R. (2001) Fruiting body formation by *Bacillus subtilis*. *Proc. Natl. Acad. Sci. U. S. A.* 98, 11621–11626.
- (5) Ma, D., Amonlirdviman, K., Raffard, R. L., Abate, A., Tomlin, C. J., and Axelrod, J. D. (2008) Cell packing influences planar cell polarity signaling. *Proc. Natl. Acad. Sci. U. S. A.* 105, 18800–18805.
- (6) Gorfinkiel, N., Blanchard, G. B., Adams, R. J., and Arias, A. M. (2009) Mechanical control of global cell behaviour during dorsal closure in *Drosophila*. *Development* 136, 1889–1898.
- (7) Dupuy, L., Mackenzie, J., and Haseloff, J. (2010) Coordination of plant cell division and expansion in a simple morphogenetic system. *Proc. Natl. Acad. Sci. U. S. A.* 107, 2711–2716.
- (8) Boyer, D., Mather, W., Mondragón-Palomino, O., Orozco-Fuentes, S., Danino, T., Hasty, J., and Tsimring, L. S. (2011) Buckling instability in ordered bacterial colonies. *Phys. Biol.* 8, 026008.
- (9) Peruani, F., Starruss, J., Jakovljevic, V., Søgaard-Andersen, L., Deutsch, A., and Bär, M. (2012) Collective motion and non-equilibrium cluster formation in colonies of gliding bacteria. *Phys. Rev. Lett.* 108, 098102.
- (10) Gardner, T. S., Cantor, C. R., and Collins, J. J. (2000) Construction of a genetic toggle switch in *Escherichia coli*. *Nature* 403, 339–342.
- (11) Tamsir, A., Tabor, J. J., and Voigt, C. A. (2011) Robust multicellular computing using genetically encoded NOR gates and chemical ‘wires’. *Nature* 469, 212–215.
- (12) Elowitz, M. B., and Leibler, S. (2000) A synthetic oscillatory network of transcriptional regulators. *Nature* 403, 335–338.
- (13) Locke, J. C. W., and Elowitz, M. B. (2009) Using movies to analyse gene circuit dynamics in single cells. *Nat. Rev. Microbiol.* 7, 383–392.

- (14) Munsky, B., Neuert, G., and Oudenaarden, A. V. (2012) Using gene expression noise to understand gene regulation. *Science* 336, 183–187.

- (15) Dunlop, M. J., Cox, R. S., Levine, J. H., Murray, R. M., and Elowitz, M. B. (2008) Regulatory activity revealed by dynamic correlations in gene expression noise. *Nat. Genet.* 40, 1493–1498.

- (16) Isalan, M., Lemerle, C., Michalodimitrakis, K., Horn, C., Beltrao, P., Raineri, E., Garriga-Canut, M., and Serrano, L. (2008) Evolvability and hierarchy in rewired bacterial gene networks. *Nature* 452, 840–845.

- (17) Garcia-Ojalvo, J., Elowitz, M. B., and Strogatz, S. H. (2004) Modeling a synthetic multicellular clock: Repressilators coupled by quorum sensing. *Proc. Natl. Acad. Sci. U. S. A.* 101, 10955–10960.

- (18) Danino, T., Mondragón-Palomino, O., Tsimring, L., and Hasty, J. (2010) A synchronized quorum of genetic clocks. *Nature* 463, 326–330.

- (19) Prindle, A., Samayoa, P., Razinkov, I., Danino, T., Tsimring, L. S., and Hasty, J. (2012) A sensing array of radically coupled genetic ‘biopixels’. *Nature* 481, 39–44.

- (20) Basu, S., Gerchman, Y., Collins, C. H., Arnold, F. H., and Weiss, R. (2005) A synthetic multicellular system for programmed pattern formation. *Nature* 434, 1130–1134.

- (21) Sprinzak, D., and Elowitz, M. B. (2005) Reconstruction of genetic circuits. *Nature* 438, 443–448.

- (22) Aranson, I. S., and Tsimring, L. S. (2006) Patterns and collective behavior in granular media: Theoretical concepts. *Rev. Mod. Phys.* 78, 641–692.

- (23) Matsushita, M., and Fujikawa, H. (1990) Diffusion-limited growth in bacterial colony formation. *Phys. A* 168, 498–506.

- (24) Budrene, E. O., and Berg, H. C. (1995) Dynamics of formation of symmetrical patterns by chemotactic bacteria. *Nature* 376, 49–53.

- (25) Volfson, D., Cookson, S., Hasty, J., and Tsimring, L. S. (2008) Biomechanical ordering of dense cell populations. *Proc. Natl. Acad. Sci. U. S. A.* 105, 15346–15351.

- (26) Asally, M., Kittisopikul, M., Rué, P., Du, Y., Hu, Z., Çağatay, T., Robinson, A. B., Lu, H., Garcia-Ojalvo, J., and Süel, G. M. (2012) Localized cell death focuses mechanical forces during 3D patterning in a biofilm. *Proc. Natl. Acad. Sci. U. S. A.* 109, 18891–18896.

- (27) Rudge, T. J., Steiner, P. J., Phillips, A., and Haseloff, J. (2012) Computational modeling of synthetic microbial biofilms. *ACS Synth. Biol.* 1, 345–352.

- (28) Koch, A. L. (1995) *Bacterial Growth and Form*, Chapman & Hall, New York.

- (29) Wang, P., Robert, L., Pelletier, J., Dang, W. L., Taddei, F., Wright, A., and Jun, S. (2010) Robust growth of *Escherichia coli*. *Curr. Biol.* 20, 1099–1103.

- (30) Kleerebezem, M., Quadri, L. E. N., Kuipers, O. P., and deVos, W. M. (1997) Quorum sensing by peptide pheromones and two-component signal-transduction systems in Gram-positive bacteria. *Mol. Microbiol.* 24, 895–904.

- (31) Costerton, J. W., Lewandowski, Z., Caldwell, D. E., Korber, D. R., and Lappin-Scott, H. M. (1995) Microbial biofilms. *Annu. Rev. Microbiol.* 49, 711–745.

- (32) Purcell, E. M. (1977) Life at low Reynolds number. *Am. J. Phys.* 45, 3–11.

- (33) Begg, K. J., and Donachie, W. D. (1998) Division planes alternate in spherical cells of *Escherichia coli*. *J. Bacteriol.* 180, 2564–2567.

- (34) de Pedro, M. A., Donachie, W. D., Höltje, J.-V., and Schwarz, H. (2001) Constitutive septal murein synthesis in *Escherichia coli* with impaired activity of the morphogenetic proteins RodA and penicillin-binding protein 2. *J. Bacteriol.* 183, 4115–4126.

- (35) Tabor, J. J., Salis, H. M., Simpson, Z. B., Chevalier, A. A., Levskaya, A., Marcotte, E. M., Voigt, C. A., and Ellington, A. D. (2009) A synthetic genetic edge detection program. *Cell* 137, 1272–1281.

- (36) Gibson, D. G., Young, L., Chuang, R.-Y., Venter, J. C., Hutchison, C. A., and Smith, H. O. (2009) Enzymatic assembly of DNA molecules up to several hundred kilobases. *Nat. Methods* 6, 343–345.

(37) Jürgen, B., Schweder, T., and Hecker, M. (1998) The stability of mRNA from the *gsiB* gene of *Bacillus subtilis* is dependent on the presence of a strong ribosome binding site. *Mol. Gen. Genet.* 258, 538–545.

(38) Veening, J.-W., Smits, W. K., Hamoen, L. W., Jongbloed, J. D. H., and Kuipers, O. P. (2004) Visualization of differential gene expression by improved cyan fluorescent protein and yellow fluorescent protein production in *Bacillus subtilis*. *Appl. Environ. Microbiol.* 70, 6809–6815.

(39) Schindelin, J., et al. (2012) Fiji: an open-source platform for biological-image analysis. *Nat. Methods* 9, 676–682.

(40) Schneider, C. A., Rasband, W. S., and Eliceiri, K. W. (2012) NIH Image to ImageJ: 25 years of image analysis. *Nat. Methods* 9, 671–675.

(41) Bérubé, D., and Jébrak, M. (1999) High precision boundary fractal analysis for shape characterization. *Comput. Geosci.* 25, 1059–1071.